JOURNAL OF SOLID STATE CHEMISTRY 31, 197–207 (1980)

Magnetic Properties and Structures of Equiatomic Rare Earth–Platinum Compounds *R*Pt (*R* = Gd, Tb, Dy, Ho, Er, Tm)

A. CASTETS AND D. GIGNOUX

Laboratoire Louis Néel, CNRS, 166X, 38042 Grenoble Cedex, France

AND J. C. GOMEZ-SAL

Departamento de Fisica Fundamental, Facultad de Ciencias, Santander, Spain

Received January 3, 1979

The magnetic properties and structures of *R*Pt compounds (*R* = Gd, Tb, Dy, Ho, Er, and Tm) are presented. Below their Curie temperature the compounds exhibit ferromagnetic behavior. In GdPt, the spontaneous magnetization at 4.2°K (6.7 μ_B/Gd) and the small superimposed susceptibility suggest that the gadolinium moments are parallel and the exchange interactions are positive. In the three types of noncollinear magnetic structures observed in the other compounds the rare earth atoms are divided into two sublattices with different magnetization directions. They give rise to a ferromagnetic component associated with an antiferromagnetic component. These structures, which are analyzed in terms of crystal field effects, result from a competition between a magnetocrystalline anisotropy and positive exchange interactions of Heisenberg type.

Introduction

The equiatomic rare earth–platinum compounds *R*Pt crystallize in the orthorhombic FeB-type structure (*1*). This structure can be built up from trigonal prisms, where the corners are occupied by rare earth atoms and the center is occupied by a platinum atom (Fig. 1). Platinum does not contribute to the magnetism of the compounds because the 5*d* shell is full. The magnetic ordering is essentially due to indirect interactions between rare earth atoms occurring through the conduction electrons. Ordering temperatures are below room temperature. Because of the arrangement in prisms, rare earth atoms lie in low symmetry sites, and the crystal field effects split totally the ground state multiplet of the non-Kramers ions or give rise to doublets. Because of the spin–orbit coupling the magnetocrystalline anisotropy is very high. As already observed in the isomorphous compounds *R*Ni (*2, 3*), the competition between these two effects (exchange and magnetocrystalline anisotropy) gives rise to unusual magnetization processes and to complex magnetic structures.

In this paper we present the magnetic properties and magnetic structures of the *R*Pt compounds with *R* = Gd, Tb, Dy, Ho, Er, and Tm.

Experimental

The rare earth elements used were 99.9% pure, and the platinum was 99.99% pure. Polycrystalline samples were induction melted in a cold crucible. For each compound the FeB-type structure was obtained.

0022-4596/80/020197-11$02.00/0

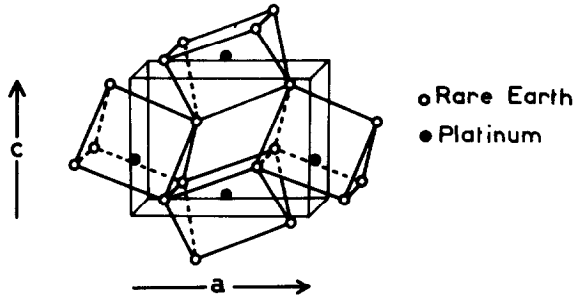

FIG. 1. Crystallographic structure of *R*Pt compounds.

Magnetic measurements between 4.2 and 300°K were performed at the SNCI (Service National des Champs Intenses, Grenoble) in fields up to 150 kOe. Magnetic structures were studied at the Laboratoire de Diffraction Neutronique du Centre d'Etudes Nucléaires de Grenoble (the neutron wavelength used on the diffraction spectrometer DN5 was 1.016 Å) and at the Institut Laue–Langevin (the neutron wavelength used on the D2 spectrometer was 1.22 Å).

Crystallographic Structure

The FeB-type crystallographic structure of the *R*Pt (*R* = rare earth) compounds belongs to the *Pnma* (D_{2h}^{16}) space group. We have determined the parameters of the orthorhombic cell for each compound (Table I). They are in good agreement with those determined by Dwight *et al.* (*1*). The crystallographic cell contains four rare earth and four platinum atoms which are in the same (4*c*) site with *m* (*Cs*) symmetry. The positions of these four atoms are: (1) in $|x, \frac{1}{4}, z|$, (2) in $|-x, \frac{3}{4}, -z|$, (3) in $|\frac{1}{2}-x, \frac{3}{4}, \frac{1}{2}+z|$, and (4) in $|\frac{1}{2}+x, \frac{1}{4}, \frac{1}{2}-z|$. From the intensities of the neutron diffraction data performed above the ordering temperature in each compound, we have refined the atomic positions of the rare earth and platinum atoms. As an example the results obtained in TbPt are shown in Table II.

TABLE I

PARAMETERS OF THE ORTHORHOMBIC CELL IN *R*Pt COMPOUNDS

	a (Å)	*b* (Å)	*c* (Å)
GdPt	7.088	4.499	5.591
TbPt	7.013	4.49	5.564
DyPt	6.974	4.479	5.542
HoPt	6.932	4.465	5.528
ErPt	6.906	4.451	5.509
TmPt	6.855	4.446	5.496

Magnetic Measurements

In Fig. 2 are shown for all the compounds studied the first magnetization curves performed at 4.2°K. In low fields they exhibit a ferromagnetic behavior. In fields higher than 20 kOe a superimposed susceptibility is observed. in all compounds except GdPt the high anisotropy of the rare earth atoms is responsible for the high superimposed susceptibility. A 150-kOe applied magnetic field is not enough to obtain the rare earth free ion value. The magnetization curves of

TABLE II

POSITIONS OF THE FOUR TERBIUM AND FOUR PLATINUM ATOMS IN TbPt[a]

	x	*y*	*z*
Tb	0.0334	0.25	0.662
Pt	0.177	0.25	0.148

[a] The positions of the four atoms are: (1) in $|x, \frac{1}{4}, z|$, (2) in $|-x, \frac{3}{4}, -z|$, (3) in $|\frac{1}{2}-x, \frac{3}{4}, \frac{1}{2}+z|$, and (4) in $|\frac{1}{2}+x, \frac{1}{4}, \frac{1}{2}-z|$.

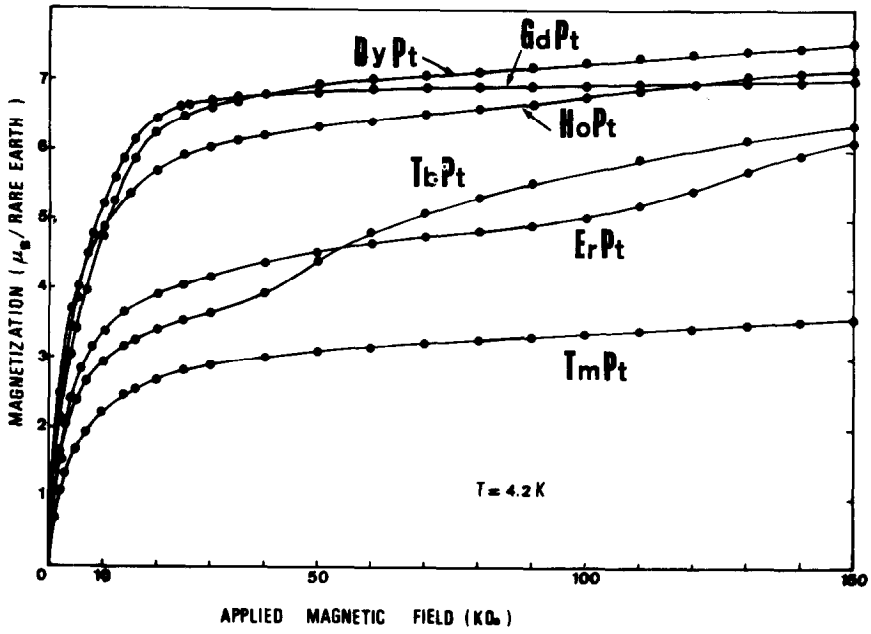

FIG. 2. First magnetization curves at 4.2°K in RPt compounds.

TbPt and ErPt exhibit transitions at 42 and 110 kOe, respectively.

The GdPt magnetization curve at 4.2°K shows together a very small superimposed susceptibility (0.9×10^{-2} emu/mole) and a spontaneous magnetization very close to the free ion value. In 150 kOe the magnetization is equal to the gadolinium free ion (7 μ_B/Gd) value. The thermal variation of the spontaneous magnetization of GdPt which is in good agreement with the Brillouin function $B_{7/2}$ is reported together with its reciprocal susceptibility in Fig. 3. These results suggest a ferromagnetic collinear arrangement of the gadolinium magnetic moments. A negative polarization of the conduction electrons is

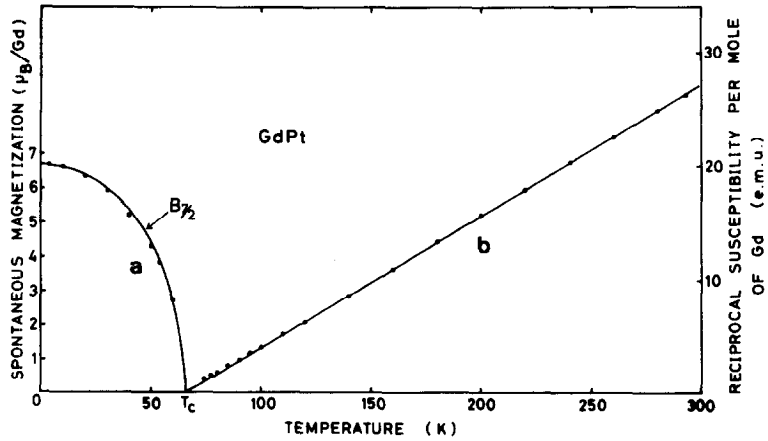

FIG. 3. GdPt. (a) Thermal variation of the spontaneous magnetization; solid circles are the experimental points, solid lines represent the $B_{7/2}$ Brillouin function. (b) Thermal variation of the reciprocal susceptibility.

responsible for the Gd magnetization reduction.

Above their Curie temperature T_c (Table III) the thermal variation of the reciprocal susceptibility of all compounds follows a Curie–Weiss law. The paramagnetic Curie temperatures Θ_p obtained are reported in Table III. The effective moments deduced from the Curie constant are in good agreement with the free ion values.

TABLE III

MAGNETIC PROPERTIES OF THE *R*Pt COMPOUNDS

Compound	Θ_p (°K)	T_c (°K)	μ_{eff} (μ_B)	$g_J\sqrt{J(J+1)}$
GdPt	66	66	8.29	7.94
TbPt	44	56	9.71	9.70
DyPt	25	23	10.45	10.60
HoPt	15	16	10.24	10.60
ErPt	14	16	9.13	9.60
TmPt	2	6	7.36	7.60

Neutron Diffraction Results

In order to determine the magnetic structure of these compounds, neutron diffraction patterns have been performed at 4.2 and 77°K. This last temperature has been chosen because it is higher than the highest Curie

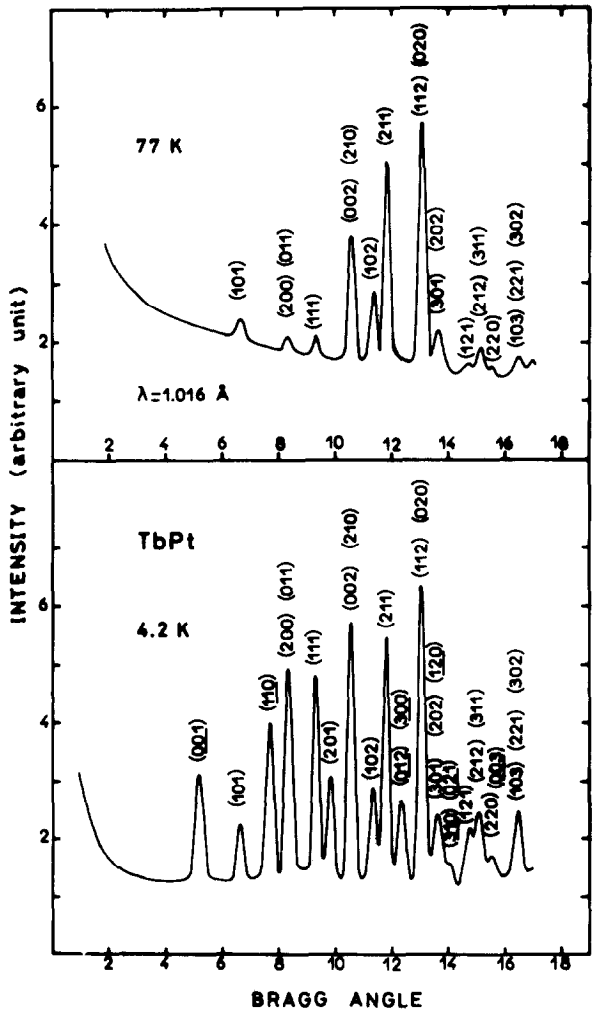

FIG. 4. TbPt: neutron diffraction patterns at 77 and 4.2°K.

temperature. (Because the absorption cross section of gadolinium $\sigma = 20\,000$ barns with $\lambda = 1.018$ Å the compound GdPt has not been studied.)

Three types of magnetic structures were observed.

(a) TbPt and DyPt

The neutron diffraction patterns of TbPt obtained at 4.2 and 77°K are shown in Fig. 4. At 77°K the intensities of the Bragg peaks are characteristic of the crystallographic structure (Fig. 1 and Table I). Especially the Bragg peaks ($h\,k\,0$) with $h = 2n+1$ (n is an integer) and ($0\,k\,l$) with $k+l = 2n+1$ do not appear. This is in agreement with the selection rules of the crystallographic space group. The nuclear intensities calculated with the atomic parameters shown in Table I are compared with the experimental values in Table IV. The discrepancy factor $R = |\sum I_{obs} - I_{cal}|/\sum I_{obs}$ is equal to 5.9%.

At 4.2°K the neutron diffraction pattern exhibits both an increase in intensity of most of the nuclear reflections and the appearance of superstructure peaks which can be indexed in the same orthorhombic cell ((100), (110), . . . , for example). Then the extinction conditions limiting the possible

TABLE IV

OBSERVED AND CALCULATED NEUTRON DIFFRACTION INTENSITIES AT 77 AND 4.2°K in TbPt

		77°K[a]		4.2°K[b]		
$h\,k\,l$	Θ	$I_{N\,cal}$	$I_{N\,obs}$	$I_{M\,cal}$	$(I_M + I_N)_{cal}$	I_{obs}
0 0 1	5.20	0.0	n.o.	19.0	19.0	22.4
1 0 1	6.70	5.2	6.0	12.5	17.7	17.9
1 1 0	7.20	0.0	n.o.	55.5	55.5	52.4
2 0 0 0 1 1	8.33 8.36	7.5	7.3	90.2	97.7	98.4
1 1 1	9.35	11.4	10.1	98.8	110.3	106.4
2 0 1	9.85	1.4	n.o.	68.8	70.3	61.8
0 0 2 2 1 0	10.52 10.59	73.5	76.1	87.6	161.2	164.6
1 0 2	11.35	42.2	47.6	22.0	64.2	70.1
2 1 1	11.80	153.5	157.9	37.7	191.2	193.4
0 1 2	12.40	0.0	n.o.	68.2	68.2	65.3
0 2 0 1 1 2	13.07 13.10	255.4	261.9	71.7	327.2	325.5
2 0 2 3 0 1 1 2 0	13.47 13.63 13.74	48.6	41.1	54.0	102.7	110.0
0 2 1 3 1 0	14.12 14.18	0.0	n.o.	23.8	23.8	30.3
1 2 1	14.75	10.3	8.0	65.3	75.7	85.6
2 1 2 3 1 1	15.01 15.15	33.1	29.2	83.7	116.9	123.6
2 2 0	15.55	10.0	11.1	35.5	45.5	42.0
0 0 3	15.90	0.0	n.o.	24.9	24.9	23.2
1 0 3 3 0 2 2 2 1	16.46 16.48 16.48	33.6	30.1	102.4	136.0	143.3

[a] $R = 5.9\%$.
[b] $R = 4.5\%$.

reflections of the *Pnma* space group are no longer valid. These superstructure lines are characteristic of an antiferromagnetic arrangement of the component along **a** of the terbium magnetic moment. Following Bertaut (*4*) this arrangement is written $-C_a = -M_{1a} - M_{2a} + M_{3a} + M_{4a}$. The increase of nuclear peaks is due to a ferromagnetic arrangement of the component along **c** of the terbium magnetic moment (written $F_c = M_{1c} + M_{2c} + M_{3c} + M_{4c}$). Thus the magnetic structure is noncollinear with the moments lying in the (010) plane. The best agreement (the discrepancy factor is $R = 4.1\%$) between the observed and the calculated intensities is obtained with no magnetic moment on platinum atoms and a moment on terbium atoms for which the characteristics are summarized in Table V. The projection of the magnetic structure in the (010) plane is shown in Fig. 5.

The DyPt and TbPt magnetic structures are isomorphous and belong to the magnetic space group *Pn'm'a*. The characteristics of the Dy moment are reported in Table V.

(*b*) *HoPt*

The diffraction data obtained at 77 and 4.2°K on polycrystalline HoPt are shown in Fig. 6. As for TbPt, at 4.2°K we observe together an increase of the nuclear Bragg reflections and the existence of superstructure peaks. However, in HoPt the superstructure Bragg peaks are different. For example, in HoPt the (001) peak is null, but we observe the (110) reflections. Then the magnetic structure is noncollinear with a ferromagnetic arrangement F_a of the holmium magnetic moment component parallel to the **a**-axis and an antiferromagnetic arrangement $-C_c$ of the component parallel to the **c**-axis. The observed and calculated intensities are compared in Table VI. The characteristics of the holmium moment and the projection of the magnetic structure in the (010) plane are in Table V and Fig. 5, respectively. We may note that HoPt and HoNi (*5*) are isomorphous and belong to the magnetic space group *Pnm'a'*.

(*c*) *ErPt and TmPt*

The neutron diffraction patterns performed on ErPt at 4.2 and 77°K are drawn in Fig. 7. At 4.2°K we observe the same superstructure peaks as in HoPt together with an increase in nuclear reflections. However, their relative intensities are different. The refinement of the observed intensities (Table VII) leads to a magnetic structure associated with the F_a and C_c arrangement. As in the previous case the magnetic structure is noncollinear with the magnetic moments

TABLE V

MAGNETIC STRUCTURE OF THE *R*Pt COMPOUNDS TOGETHER WITH THE CHARACTERISTICS OF THE MOMENT OF THE RARE EARTH IN POSITION (1)

Compound	Magnetic arrangement	Magnetic space group	μ_{obs} (μ_B)	μ_{cal} (μ_B)	Rotation angle Θ_c (degrees)	Observed angle with **a** axis, Ψ_{obs} (degrees)	Calculated angle with **a** xis, Ψ_{cal} (degrees)
GdPt							
TbPt	$-C_a, -, F_c$	*Pn'm'a*	8.1	8.5	−39	−128	−129
DyPt	$-C_a, -, F_c$	*Pn'm'a*	7.1	8.9	−39	−134	−129
HoPt	$F_a, -, -C_c$	*Pnm'a'*	8.2	9.5	−43	23	47
ErPt	$F_a, -, C_c$	*Pnm'a'*	8.1	8.7	−45	−18	−45
TmPt	$F_a, -, C_c$	*Pnm'a'*	4.5	7.0	−37	−37	−37

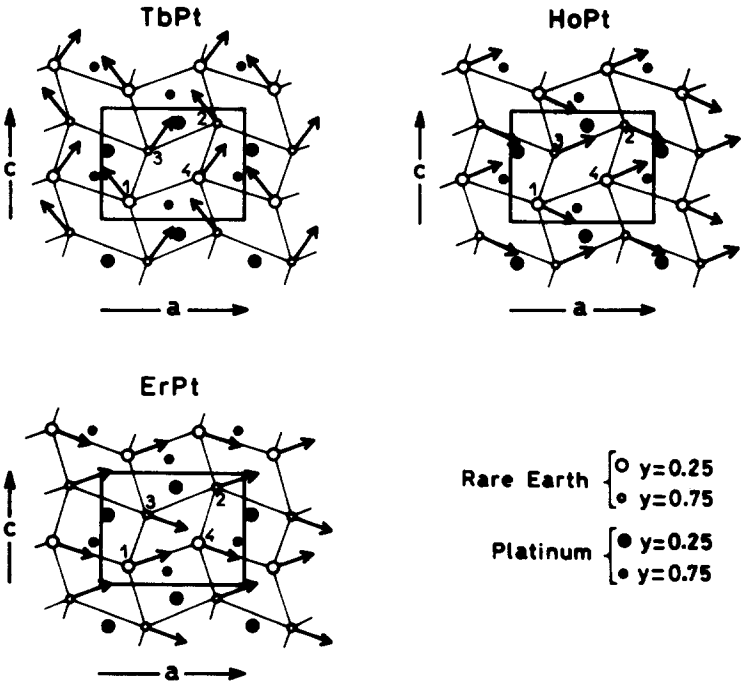

FIG. 5. Projection of the magnetic structures of TbPt, HoPt, and ErPt in the (a, c) planes.

lying in the (010) plane (Fig. 8). This structure is isomorphous to that of TmPt and belongs to the same magnetic group as HoPt (*Pnm'a'*) but the direction of the magnetic moments is different (Table V).

Discussion

In the compounds we have studied rare earth ions lie in a site with very low symmetry because the only symmetry element is a mirror plane perpendicular to **b**. The crystal field Hamiltonian acting on the ground state multiplet of the R^{3+} ion can be written, in the axis system where $0x$ is parallel to **c**, $0y$ parallel to **a**, and $0z$ parallel to **b**:

$$\mathcal{H}_c = \alpha_J(V_2^0O_2^0 + V_2^2O_2^2 + V_2^{-2}O_2^{-2}) + \beta_J \sum_{m=2n=-4}^{+4} V_4^mO_4^m + \gamma_J \sum_{m=2n=-6}^{+6} V_6^mO_6^m.$$

The O_1^m are the Stevens equivalent operators (*6*); they are angular momentum operator functions of J_x, J_y, and J_z. The V_1^m are a development of the local electric potential, and α_J, β_J, and γ_J describe the $4f$ multipoles of the ion. The second-order terms, which are dominant, express the interactions between the quadrupole of the surrounding atoms and that of the $4f$ shell. By making a coincidence between the principal axes of the quadrupole of the surrounding atoms and our system axis, it is possible to write the quadrupolar term in a canonical form. Then the second-order term becomes $\alpha_J(V_0^2O_2^2 + V_2^2O_2^2)$. In our case, this coincidence can be obtained by a rotation around the $0z$ axis with angle Θ_c, such that (*7*) $\tan 2\Theta_c = V_2^{-2}/V_2^2$. With the help of a point charge model, we can calculate the V_1^m parameters. This model allows us to express quantitatively the surrounding potential form. In this case, the calculated second-order terms are generally dominant and are in good agreement with those obtained experimentally. We have taken a charge of $+3e$ for R^{3+}

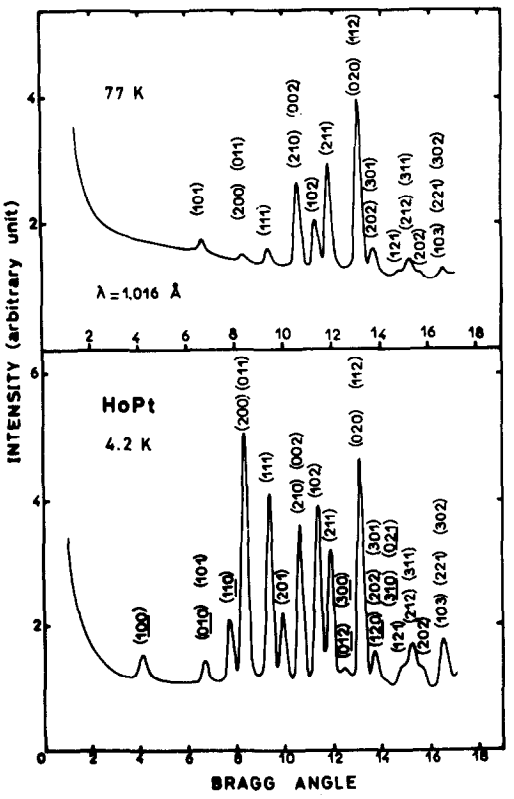

FIG. 6. HoPt: neutron diffraction patterns at 77 and 4.2°K.

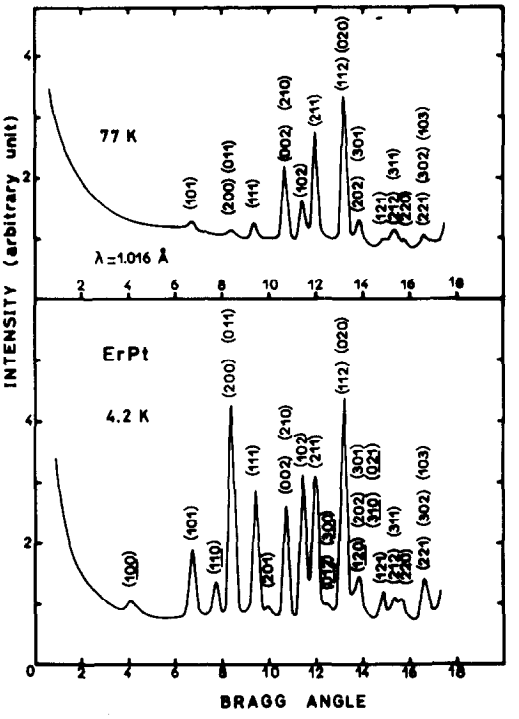

FIG. 7. ErPt: neutron diffraction patterns at 77 and 4.2°K.

ions and we have assumed a zero charge on platinum atoms. The rotation angles obtained, Θ_c, are listed in Table V.

In the new axis system $0x'y'z$, obtained after rotation (Fig. 8) the second-order term of the crystal field Hamiltonian can be written simply:

$$\mathcal{H}_c = \alpha_J (A_{x'} J_{x'}^2 + A_{y'} J_{y'}^2 + A_{z'} J_{z'}^2).$$

In the TbPt compound, for example, $A_{x'} = 88.3$, $A_{y'} = -115.4$, and $A_{z'} = 27.1\ \text{cm}^{-1}$. These values, which are characteristic of the surrounding atoms, change very little between different *R*Pt compounds. This is not true for α_J which differs from one rare earth ion to another. In particular, α_J is negative for Tb, Dy, and Ho ions, and positive for Er and Tm ions.

If J is large ($J \geq 6$), and if the three A_i factors ($i = x', y', z'$) are very different, conditions which are satisfied in *R*Pt compounds, Fert and Campbell (*8*) have shown that for any rare earth ion (Kramers or not) the ground state due to the crystal field is a doublet for which the corresponding eigenfunctions are quasi-pure states $|J_i> = |\pm J>$ ($i = x', y', z'$). Therefore, a semiclassical treatment is possible: If we consider J_i

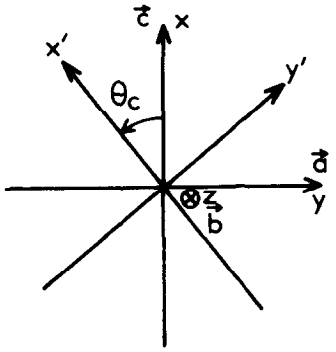

FIG. 8. Reference axes before ($0xyz$) and after rotation ($0x'y'z'$).

TABLE VI

OBSERVED AND CALCULATED NEUTRON DIFFRACTION INTENSITIES AT 77 AND 4.2°K IN HoPt

		77°K[a]		4.2°K[b]		
$h\,k\,l$	Θ	$I_{N\,\mathrm{cal}}$	$I_{N\,\mathrm{obs}}$	$I_{M\,\mathrm{cal}}$	$(I_M+I_N)_{\mathrm{cal}}$	I_{obs}
1 0 0	4.20	0.0	n.o.	3.7	3.7	4.3
1 0 1	6.75	9.0	7.1	0.0	9.0	10.5
1 1 0	7.77	0.0	n.o.	32.9	32.9	35.1
0 1 1 2 0 0	8.409 8.42	2.2	5.4	160.1	162.4	161.3
1 1 1	9.41	14.7	16.1	108.5	123.2	130.7
2 0 1	9.96	0.9	1.1	45.5	46.4	53.9
0 0 2 2 1 0	10.59 10.69	81.9	76.1	61.1	143.1	147.5
1 0 2	11.41	65.4	60.9	127.3	192.8	200.3
2 1 1	11.94	153.5	149.7	44.8	198.3	185.5
0 1 2 3 0 0	12.48 12.70	0.0	n.o.	21.9	21.9	22.2
0 2 0 1 1 2	13.15 13.59	302.2	304.8	129.2	431.5	433.6
2 0 2 3 0 1 1 2 0	13.59 13.78 13.83	56.5	61.8	7.4	63.9	58.2
0 2 1 3 1 0	14.20 14.33	0.0	n.o.	9.7	9.7	6.5
1 2 1 2 1 2 3 1 1 2 2 0	14.83 15.13 15.31 15.70	75.2	74.0	176.9	252.2	238.4
1 0 3 2 2 1 3 0 2	16.57 16.60 16.65	27.4	28.8	135.8	163.3	157.1

[a] $R = 4.8\%$.
[b] $R = 4.1\%$.

as the components of a J vector, the energy is minimum when this vector is parallel to the i-axis associated with the lowest coefficient $\alpha_J A_i$. In RPt compounds, we can easily show that the magnetization is along the $0x'$ direction in TbPt, DyPt, and HoPt ($\alpha_J < 0$) and along the $0y'$ direction in ErPt and TmPt ($\alpha_J > 0$), that is to say, perpendicular to the $0x'$ direction. In our calculation, it is possible to take into account the fourth- and sixth-order crystal field terms. In this case, the minimum of the crystal field Hamiltonian is obtained for directions very close to the previous ones. In Table V we compare the calculated and experimental magnetic moments (modulus and direction) of the ion in the (1) crystallographic position (Fig. 5). Despite the oversimplified model, the agreement is good. The differences can be attributed to fourth- and sixth-order crystal field terms which are larger than those calculated in the point charge model, a fact which has previously been noted by several authors (*9–11*). In fact, in HoPt and ErPt the agreement is not so good. In these compounds, the α_J are weaker and consequently the second-order terms are no longer dominant. The Ψ_{obs} angles between the moments and the a-axis

TABLE VII

OBSERVED AND CALCULATED NEUTRON DIFFRACTION INTENSITIES AT 77 AND 4.2°K IN ErPt

		77°K[a]		4.2°K[b]		
$h\,k\,l$	Θ	$I_{N\,cal}$	$I_{N\,obs}$	$I_{M\,cal}$	$(I_M+I_N)_{cal}$	I_{obs}
1 0 0	4.22	0.0	n.o.	1.9	1.9	3.0
1 0 1	6.77	7.3	6.9	26.5	33.8	34.3
1 1 0	7.80	0.0	n.o.	21.8	21.8	21.0
0 1 1 2 0 0	8.44 8.46	3.3	3.7	145.6	148.9	149.0
1 1 1	9.45	11.4	10.3	106.4	117.9	127.4
2 0 1	10.00	0.0	n.o.	6.3	6.4	4.8
0 0 2 2 1 0	10.63 10.73	77.8	77.4	45.0	122.8	127.6
1 0 2	11.45	57.2	56.5	139.1	196.3	185.6
2 1 1	11.99	154.0	157.7	90.7	244.7	239.2
0 1 2 3 0 0	12.53 12.75	0.0	n.o.	13.8	13.8	14.0
0 2 0 1 1 2	13.19 13.24	259.9	264.4	143.9	403.9	395.0
2 0 2 3 0 1 1 2 0	13.65 13.84 13.88	42.5	45.4	34.4	77.0	70.4
0 2 1 3 1 0	14.25	0.0	n.o.	9.1	9.1	7.0
1 2 1	14.89	14.7	8.1	37.1	51.9	54.0
2 1 2 3 1 1 2 2 0	15.19 15.37 15.76	59.9	60.5	75.1	135.1	125.5
1 0 3 2 2 1 3 0 2	16.63 16.67 16.71	31.0	28.4	84.2	115.2	114.1

[a] $R = 3.3\%$.
[b] $R = 3.9\%$.

(Table V) are then inferior to 45°, which is a value far from that calculated. The weak value of the observed moment in TmPt arises from the small difference between the ordering temperature ($T_c = 6$°K) and the temperature of the neutron diffraction experiment (4.2°K).

The magnetic moment direction of the other rare earth ions in the elementary cell are deduced from the ion in position (1) by the symmetry operators of the *Pnma* space group. The moments are then divided into two sublattices with different magnetization directions. This is in agreement with the noncollinear arrangements observed experimentally. Thus the observed magnetic structures result, as in the *R*Ni (*2, 3*) and *R*Al (*12*) compounds, from a competition between the exchange interactions and the magnetocrystalline anisotropy. This last anisotropy divides the rare earth ions into two sublattices with different magnetization directions.

However, except in the case of HoPt, the magnetic structures of *R*Pt compounds are different from those of *R*Ni. In particular, the

directions of the ferromagnetic components are not the same. It is along **c** in DyPt and along **a** in DyNi. These differences come from the variation of the surroundings: The platinum atom is much bigger than the nickel atom and the ratio c/a goes from 0.77 in *R*Ni to 0.79 in *R*Pt. Consequently the quadrupole of the surrounding atoms is modified. Thus, in the *R*Ni compounds, the quadrupole directions are obtained after a rotation of about −51°, while in the *R*Pt compounds a rotation of −39° is enough. These two angles being on either side of the $-\Pi/4$ value the direction of the ferromagnetic components must be different for *R*Ni and *R*Pt compounds. For the rare earth ions in which $\alpha_J < 0$ this direction is parallel to **a** in *R*Ni compounds and parallel to **c** in *R*Pt compounds. For the rare earth ions in which $\alpha_J > 0$, this direction is parallel to **c** in *R*Ni compounds and parallel to **a** in *R*Pt compounds. However, HoPt is an exception, because the second-order crystal field terms are no longer dominant. Then the direction of the Holmium moment makes an angle of 23° with the **a**-axis instead of 47°, which is the calculated value. The ferromagnetic component is parallel to the **a**-axis as in HoNi.

The almost isotropic behavior of the ferromagnetic GdPt compound is not surprising: The gadolinium, being in an *S* state, is not submitted to the crystal field effects. Then, only the positive exchange interactions remain. As the gadolinium atoms are not split into two sublattices, the compound is ferromagnetic collinear. Hence, the crystal field effects alone explain correctly the noncollinear arrangements observed in the other compounds. It is not necessary to take into account anisotropic exchange terms.

The transitions, observed in high fields, in the magnetization curves of the TbPt and HoPt compounds are due to the reversal, by the applied field, of the antiferromagnetic sublattice magnetization of the crystallites whose direction is of antiferromagnetism close to that of the applied field. These transitions have been studied quantitatively on *R*Ni single crystals (*13*).

Acknowledgments

We wish to thank R. Lemaire for fruitful discussions.

References

1. A. E. Dwight, R. A. Conner, and J. W. Downey, *Acta Crystallogr.* **18**, 825 (1965).
2. D. Gignoux, *J. Phys. (Paris)* **35**, 455 (1974).
3. D. Gignoux, D. Paccard, J. Rossat-Mignot, and F. Tcheou, *in* "10th Rare Earth Research Conference," Vol. II, p. 596 (1973).
4. E. F. Bertaut, *Acta Crystallogr. Sect. A* **24**, 217 (1968).
5. R. Lemaire and D. Paccard, "Les eléments de terres rares," Vol. II, p. 231 (1970).
6. M. T. Hutchings, *Solid State Phys.* **16**, 227 (1964).
7. J. Rossat-Mignod and F. Tcheou, *J. Phys. (Paris)* **33**, 423 (1972).
8. A. Fert and I. A. Campbell, *J. Phys. F* **8**, L57 (1978).
9. P. Morin, J. Pierre, J. Rossat-Mignod, K. Knorr, and W. Drexel, *Phys. Rev. B* **9**, 4932 (1974).
10. D. Gignoux, F. Givord, and R. Lemaire, *Phys. Rev. B* **12**, 3878 (1975).
11. B. Barbara, M. F. Rossignol, H. G. Purwins, and E. Walker, "Physique sous champs magnétiques intenses," Colloque International du CNRS No. 242, p. 51 (1975).
12. J. K. Yakinthos and F. Tcheou, *Solid State Commun.* **18**, 1287 (1976).
13. D. Gignoux and R. Lemaire, *Solid State Commun.* **14**, 877 (1974).